

Simulating LEO Satellite Tracking with Ground Station Antenna Dynamics and PID Control in MATLAB

Ioannis Ziargas ^{ID}, *University of the Peloponnese*⁽¹⁾
Supervisor: Georgios Souliotis ^{ID}, *University of the Peloponnese*⁽²⁾

Abstract—This paper serves as an introductory guide for beginners to the fundamental challenges of satellite communications. With the rising interest in mega satellite constellations for global internet access and the integration of Internet of Things (IoT) devices, the need for a basic understanding of this field is more critical than ever. The paper begins with orbital mechanics to explain satellite motion and transitions into ground station types and antenna dynamics, emphasizing how communication links are formed. It further addresses the derivation of a DC motor's transfer function and PID controller tuning for precise system operation. The paper concludes with a Low Earth Orbit (LEO) satellite tracking simulation that integrates these components, illustrating their practical application and interdependence in satellite communication systems.

Index Terms—Dense satellite networks, antenna dynamics, pass-duration, low earth orbit, leo satellite, control system, pid controller, DC motor

I. INTRODUCTION

As modern digital telecommunications technologies advance, the pursuit of fast and reliable global data transmission has accelerated, driving a shift toward ubiquitous high-speed connectivity. The growth of the Internet and the expansion of the Internet of Things (IoT) into industry and daily life [1] have created a soaring demand for robust and stable connections, reaching even the most remote regions, such as marine and aerial environments, where traditional terrestrial infrastructure is unfeasible. In response, the industry has turned to deploying dense satellite constellations in Low Earth Orbit (LEO), which offer a promising solution to meet the rising demand for global connectivity [2].

Leading companies, including SpaceX with its Starlink constellation [3] and EutelSat's OneWeb constellation [4], along with newer entrants like Geespace's Geely Future Mobility Satellite Constellation [5], Amazon's Project Kuiper [6] and SpaceRISE's IRIS² [7], among others, are actively developing and expanding their LEO satellite networks to provide low latency and better link capacity to meet global connectivity

⁽¹⁾The author is with the School of Electrical and Computer Engineering, University of the Peloponnese, Patras, Greece (e-mail: ece20229@go.uop.gr). This paper was submitted as the semester project for the course **Advanced Control Systems (ECE_ELE760)** during the 2024 - 2025 academic year.

⁽²⁾The supervisor, Associate Professor at the School of Electrical and Computer Engineering, University of the Peloponnese, Greece (email: gsoul@go.uop.gr), is serving as the instructor for the course **Advanced Control Systems (ECE_ELE760)** during the 2024-2025 academic year.

demands. However, due to their high orbital speeds, each satellite remains within range of any given ground station for only a brief period, creating a significant technical challenge to track these fast-moving satellites [8] and ensure an optimal connection—a challenge that will only intensify as deployment accelerates. Currently, SpaceX has 6,857 satellites in operation [9], with nearly 12,000 satellites planned to deploy [10], while OneWeb has deployed 652 satellites to date [11].

This paper explores the foundational principles of orbital mechanics and their role in satellite orbit simulations. It provides an overview of ground station types and the frequency spectrum essential for satellite communication systems. The paper also delves into antenna dynamics, detailing the derivation of a transfer function for motors used to adjust and align antennas with targeted satellites. Concluding with the design of a Proportional-Integral-Derivative (PID) controller, it highlights how such controllers enable high-precision satellite tracking with minimal error.

II. ORBITAL MECHANICS

Orbital mechanics [12], also known as astrodynamics, is the study of the motion of artificial and celestial objects under the influence of gravitational forces, atmospheric drag, solar wind, and any other effects that may be present. Rooted in classical mechanics and expanded through modern computational methods, orbital mechanics provides the theoretical framework for understanding, predicting, and controlling the trajectories of satellites, spacecraft, and other bodies in space.

The foundation of orbital mechanics lies in Newton's laws and the universal law of gravitation, but are perturbed by the effects of general relativity. These principles enable the derivation of orbital parameters, such as the semi-major axis, semi-minor axis, inclination, argument of periapsis, and the right ascension of the ascending node (RAAN), which together define the shape and orientation of an object's trajectory, as illustrated in Fig. 3. Advanced topics include perturbation analysis, account for the effects of atmospheric drag and gravitational anomalies. The latter will be explored using the SGP4 propagator later in this paper.

A. Kepler's Laws of Planetary Motion

The Kepler laws of planetary motion form a cornerstone of orbital mechanics, describing the fundamental properties of

orbital trajectories. Initially developed to explain the motion of celestial bodies, these laws are equally applicable to man-made satellites, providing a framework for calculating orbital parameters and understanding motion dynamics.

1) Law of Ellipses (First Law):

Kepler's First Law states that the orbit of a celestial body is an ellipse, with the central body (e.g. Earth) at one of its two foci. For man-made satellites, this means that their trajectories are elliptical unless altered into more circular orbits. The shape of the orbit is characterized by its eccentricity (e), defined as:

$$e = \frac{r_a - r_p}{r_a + r_p} \quad (1)$$

Where:

- r_a : Apogee distance from the Earth.
- r_p : Perigee distance from the Earth.

Alternatively, eccentricity can be determined from the semi-major axis (a) and semi-minor axis (b) as:

$$e = \sqrt{1 - \frac{b^2}{a^2}} \quad (2)$$

and

$$a = R_e + h \quad (3)$$

where:

- R_e : Earth radius.
- h : Height of the satellite.

In Fig. 1, the semi-major axis (a) is defined as the distance from the center of the ellipse to its farthest point along the longest diameter. Similarly, the semi-minor axis (b) represents the distance from the center of the ellipse to its closest point along the shortest diameter. The true anomaly (θ) is the angular distance between the satellite's current position and the perigee, measured within the orbital plane.

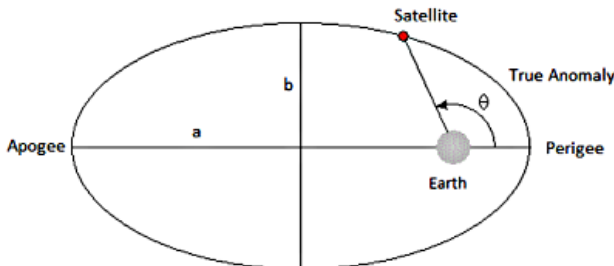


Fig. 1. The diagram illustrates a satellite in an elliptical orbit around the Earth, highlighting key orbital parameters. The semi-major axis (a) and semi-minor axis (b) define the orbit's dimensions. The true anomaly (θ) represents the satellite's angular position relative to the perigee, which is the closest point to Earth. The apogee, the farthest point from Earth, is also labeled, providing a clear depiction of the satellite's trajectory.

2) Law of Equal Areas (Second Law):

Kepler's Second Law states that a line joining an orbiting

body (e.g. a satellite) to the central body (e.g. the Earth) sweeps out equal areas in equal intervals of time. This implies that the orbital velocity of the orbiting body is not constant but varies depending on its distance from the central body. Specifically, the body moves faster when it is closer to the central body (at periapsis) and slower when it is farther away (at apoapsis) as illustrated in Fig. 2 and described by the equation for areal velocity:

$$\frac{dA}{dt} = \frac{1}{2} r^2 \frac{d\theta}{dt} \quad (4)$$

Where:

- r : Distance between the satellite and the Earth.
- $\frac{d\theta}{dt}$: Rate of change of the angular position of the satellite.

Eq. 4 demonstrates that when the distance (r) increases, the satellite is closer to the apoapsis, and the angular velocity ($\frac{d\theta}{dt}$) decreases to maintain constancy. Alternatively, when the distance (r) decreases, the satellite is closer to the perapsis, and the angular velocity ($\frac{d\theta}{dt}$) increases to ensure that the term ($r^2 \frac{d\theta}{dt}$) remains constant. This constancy preserves the areal velocity, meaning the satellite sweeps out equal areas in equal times. Understanding this principle is essential for calculating satellite pass durations and ensuring accurate tracking in orbital mechanics.

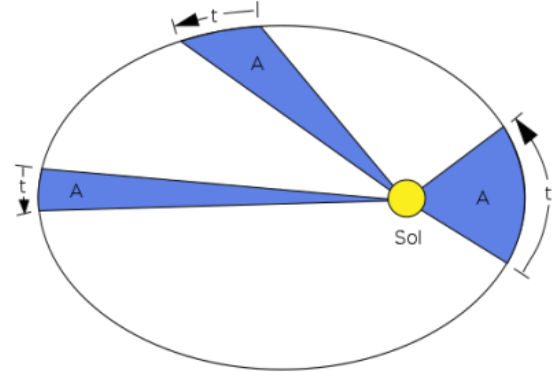


Fig. 2. The figure illustrates Kepler's Second Law, which states that a line joining an orbiting body to the central body sweeps out equal areas in equal time intervals. The blue-shaded regions ("A") show that the body moves faster near periapsis and slower near apoapsis, maintaining the conservation of angular momentum.

3) Law of Harmonies (Third Law):

Kepler's Third Law describes the time required for a celestial body to complete one full orbit around another celestial body. In our context, this law can be applied to calculate the orbital period (T) required for a satellite to complete one full cycle around the Earth.

$$T = 2\pi * \sqrt{\frac{a^3}{\mu}} \quad (5)$$

Where μ is called the standard gravitational parameter.

- For Earth $\mu = 3.986004418 * 10^{14} \left[\frac{m^3}{s^2} \right]$

These three laws are not only fundamental to understanding orbital mechanics but also form the basis for the derivation of the Keplerian elements, which provide a complete description of a satellite's orbit.

B. Keplerian Elements

Keplerian elements are a set of six parameters that fully define the size, shape, orientation and position of a satellite's orbit at any given time. These elements allow for a comprehensive description of any satellite's motion in space. They include:

- 1) **Semi-Major Axis (a):** Defines the size of the orbit and determines the satellite's orbital period.
- 2) **Eccentricity (e):** Describes the shape of the orbit, ranging from circular $e = 0$ to elliptical $0 < e < 1$ and parabola $e = 1$.
- 3) **Inclination (i):** Specifies the angle between the norm of the orbital plane and the z-axis of Earth (rotational axis of Earth).
- 4) **Right Ascension of the Ascending Node (RAAN, Ω):** Represents the angle of the rotation of the orbital plane around the z-axis of Earth.
- 5) **Argument of Periapsis (ω):** Defines the rotation of the ellipse within the orbital plane.
- 6) **True Anomaly (v):** Indicates the satellite's position along the orbit at a given time.

Knowing these elements, we can accurately compute the satellite's orbit and its trajectory in space, as shown in Fig. 3.

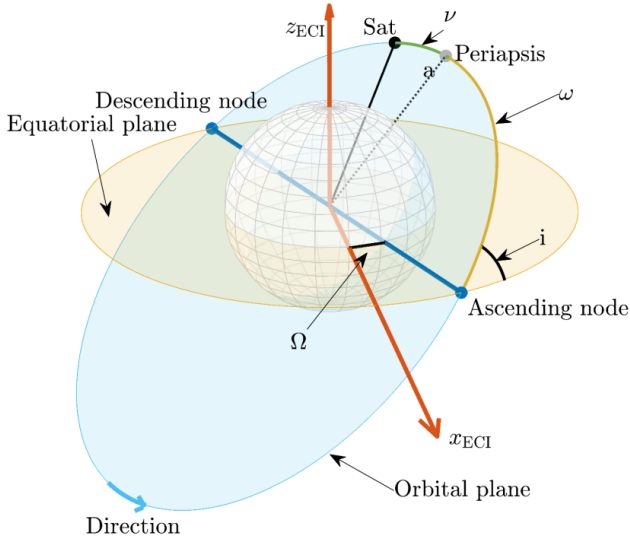


Fig. 3. The diagram illustrates the orbital parameters of a satellite in the Earth-Centered Inertial (ECI) reference frame. The orbit is shown as an elliptical trajectory in the orbital plane (blue), inclined relative to the equatorial plane (yellow) by an angle i (inclination). The diagram also marks the ascending and descending node, which are the intersection points of the orbital plane with the equatorial plane. The Earth is located at the focus of the orbit, as per Kepler's First Law. This visualization effectively demonstrates the geometric and positional elements essential for describing the satellite's orbit. The orbital parameters in this example are: $\{h = 10000 \text{ kms}, e = 0.5, i = 30^\circ, \omega = 45^\circ, \Omega = 15^\circ, v = 0^\circ\}$

C. Two-Body Propagator

The simplest method used to compute the future position and velocity of a satellite in orbit around Earth is the Two-Body Propagator. This method assumes that the satellite's motion is influenced only by Earth's gravity, neglecting other forces such as atmospheric drag, third body perturbations or Earth's oblateness.

The inputs to this method are the Keplerian elements, time elapsed vector (\vec{t}) and standard gravitational parameter (μ) with the outputs being the position vector (\vec{r}) and velocity vector (\vec{v}) in the Earth-Centered Inertial (ECI) coordinate system. To calculate the (\vec{r}) and (\vec{v}), the following steps are performed.

- 1) **Calculate the Mean Anomaly (M):** The mean anomaly is the angular distance, measured from the periapsis (the closest point in the orbit), that a fictitious body would have traveled if it moved at a constant angular velocity along a circular orbit with the same orbital period as the actual elliptical orbit as seen in Fig. 4. The mean anomaly is useful because it relates the true anomaly (the actual position of the body in its elliptical orbit) to time. Additionally, it provides a linear measure of time progression within the orbit, simplifying calculations. The mean anomaly is calculated as:

$$M = 2\pi \frac{t}{T} + M_0 \quad (6)$$

Where:

- t : Time vector.
- T : Orbital period.
- M_0 : Initial mean anomaly.

- 2) **Calculate the Eccentric Anomaly (E):** The eccentric anomaly describes the position of a satellite relative to the center of the auxiliary circle (a fictitious circle with the same semi-major axis as the elliptical orbit). It acts as a bridge between the mean anomaly and the true anomaly. The relationship between M and E is given as:

$$M = E - esin(E) \quad (7)$$

- 3) **Calculate the True Anomaly (v):** The true anomaly is the angular position of a satellite along its elliptical orbit, measured from the periapsis. It is a geometrically significant parameter that indicates the body's actual position relative to the focus of the ellipse, where the Earth is located. The true anomaly is calculated using the following equations:

$$v_x = atan2 \left(\frac{\cos(E) - e}{1 - e\cos(E)} \right) \quad (8)$$

$$v_y = atan2 \left(\frac{\sqrt{1 - e^2} \sin(E)}{1 - e\cos(E)} \right) \quad (9)$$

Where:

- v_x : True anomaly in the x-axis.

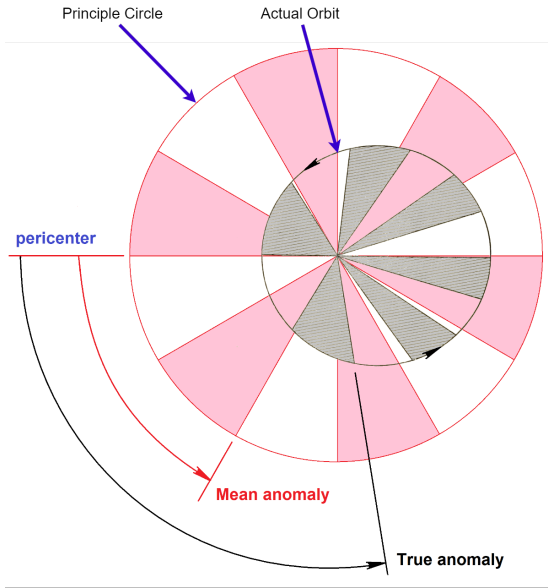


Fig. 4. This diagram compares the actual elliptical orbit (gray) of a celestial body with the principle circle (pink). The pericenter (blue) serves as the reference point for measuring the anomalies. The mean anomaly (red arrow) represents the angular distance a fictitious body would travel at constant angular velocity along the principle circle, shown by evenly divided sectors. The true anomaly (black arrow) is the angular position of the body in the elliptical orbit, reflecting its varying speed due to the orbit's shape. This figure highlights how the mean anomaly simplifies orbital calculations while the true anomaly accounts for elliptical motion.

- v_y : True anomaly in the y-axis.

4) **Calculate the Instantaneous Radius (r):** The instantaneous radius is the distance between the satellite and the Earth at a specific point at the orbit. It represents the current radial position of the satellite within its elliptical trajectory, as illustrated in Fig. 1 and explained in greater detail in Fig. 5. The equation is given by:

$$r = a(1 - e\cos(E)) \quad (10)$$

Having determined the \vec{v} and \vec{r} , we can now compute the base elliptical orbit (B_o). Since the vectors are expressed in polar coordinates, they must be converted to Cartesian coordinates. The B_o is given by:

$$B_o = \begin{bmatrix} r\cos v_x \\ r\sin v_y \\ 0 \end{bmatrix} \quad (11)$$

Where:

- $x_{orb} = r\cos v_x$
- $y_{orb} = r\sin v_y$
- $z_{orb} = 0$

Currently we have calculated the satellite's orbit in a 2D orbital plane. To represent the satellite's trajectory in a 3D ECI coordinate system, we need to apply rotational transformations based on the orbital orientation. This process involves the following Keplerian elements: $\{i, \text{RAAN}, \omega\}$.

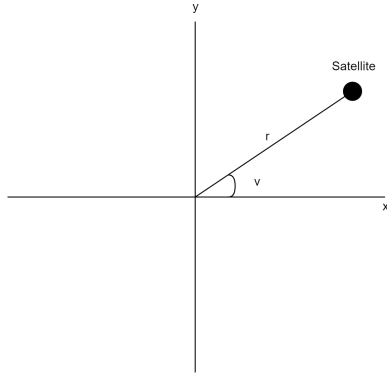


Fig. 5. This illustration shows the orbital plane of a satellite plotted in 2D Cartesian coordinates. The satellite's position in the orbit at any given moment is determined by its instantaneous radius (r) and true anomaly (v). The Earth is located at the center of the x-y axes. This plot demonstrates how (r) varies with (v), forming the elliptical trajectory.

- 1) **Rotate by ω :** Aligns the orbit within the orbital plane to match the true anomaly (z-axis).

$$\begin{bmatrix} x_1 \\ y_1 \\ z_1 \end{bmatrix} = \begin{bmatrix} \cos(\omega) & -\sin(\omega) & 0 \\ \sin(\omega) & \cos(\omega) & 0 \\ 0 & 0 & 1 \end{bmatrix} \begin{bmatrix} x_{orb} \\ y_{orb} \\ z_{orb} \end{bmatrix} \quad (12)$$

- 2) **Rotate by i :** Tilts the orbital plane relative to the equatorial plane (x-axis).

$$\begin{bmatrix} x_2 \\ y_2 \\ z_2 \end{bmatrix} = \begin{bmatrix} 1 & 0 & 0 \\ 0 & \cos(i) & -\sin(i) \\ 0 & \sin(i) & \cos(i) \end{bmatrix} \begin{bmatrix} x_1 \\ y_1 \\ z_1 \end{bmatrix} \quad (13)$$

- 3) **Rotate by the RAAN** Aligns the orbital plane to the reference direction (z-axis).

$$\begin{bmatrix} x_{ECI} \\ y_{ECI} \\ z_{ECI} \end{bmatrix} = \begin{bmatrix} \cos(\Omega) & -\sin(\Omega) & 0 \\ \sin(\Omega) & \cos(\Omega) & 0 \\ 0 & 0 & 1 \end{bmatrix} \begin{bmatrix} x_2 \\ y_2 \\ z_2 \end{bmatrix} \quad (14)$$

This simplifies to:

$$\begin{bmatrix} x_{ECI} \\ y_{ECI} \\ z_{ECI} \end{bmatrix} = R(\Omega) * R(i) * R(\omega) * \begin{bmatrix} x_{orb} \\ y_{orb} \\ z_{orb} \end{bmatrix} \quad (15)$$

Where:

- $R(\Omega)$: Rotation matrix for RAAN.
- $R(i)$: Rotation matrix for inclination.
- $R(\omega)$: Rotation matrix for the argument of periapsis.

Eq. 15 provides the satellite's 3D position in ECI coordinates for a specific time interval. By computing this position at regular intervals over a one-day period, the resulting trajectory can be used to generate the orbit, as illustrated in Fig. 3.

D. SGP4 Propagator

Because the two-body propagator is a simplistic model, real-world scenarios often require more advanced methods, such as the Simplified General Perturbations 4 (SGP4) propagator.

SGP4 is a widely used model designed to compute the position and velocity of Earth-orbiting satellites over time. It is specifically tailored for use with the Two-Line Element (TLE) set [13], a standardized format that encodes orbital parameters using a modified Keplerian framework. Unlike the two-body propagator, SGP4 accounts for key perturbation effects including:

- **Earth's Oblateness (J2 Effect):** Accounts for the Earth's equatorial bulge, which affects satellite motion by causing precession of the orbit.
- **Atmospheric Drag:** Models the deceleration experienced by low Earth orbit (LEO) satellites as they encounter atmospheric particles, leading to orbital decay.
- **Third-Body Effects:** Includes minor influences from the Sun and Moon, though less accurately than specialized models.
- **Solar Radiation Pressure:** Handles radiation pressure as a small perturbative force (simplified).

These key characteristics of SGP4 make it particularly well-suited for practical satellite tracking and prediction.

For a more in-depth analysis of the SGP4 propagator, readers are encouraged to refer to the cited source [14]. Detailing the mathematical foundation of the SGP4 algorithm falls outside the primary scope of this paper.

E. Satellite Orbit Types

Satellite orbits are categorized based on their altitude and specific mission requirements [15]. The primary types of Earth-centered orbits include low Earth orbit (LEO), medium earth orbit (MEO) and geostationary orbit (GEO) as seen in Fig. 6, each offering distinct advantages for various applications.

- **Low Earth Orbit (LEO):** LEO refers to orbits with altitudes ranging between 500 km to 900 km above the Earth's surface. Satellites in LEO experience shorter orbital periods (approximately 9 to 13 minutes) and are ideal for applications requiring high resolution imaging, low-latency communications, or global coverage via constellations. Typical examples include Earth observation satellites, the International Space Station (ISS) and satellite constellations.
- **Medium Earth Orbit (MEO):** MEO encompasses orbits with altitudes between 5,000 km to 12,000 km, placing these satellites between LEO and GEO. MEO satellites are commonly used for navigation systems such as the Global Positioning System (GPS), Galileo, and GLONASS, providing a balance between coverage, latency, and orbital stability. Orbital periods in MEO range from approximately 2 to 12 hours.
- **Geostationary Earth Orbit (GEO):** GEO refers to circular orbits located at a specific altitude of 36,000 km above the Earth's equator. Satellites in GEO have an orbital period that matches Earth's rotation (24 hours) and thus appear stationary relative to a fixed point on the Earth's surface. This characteristic makes GEO ideal for

applications such as communications, weather monitoring and broadcasting.

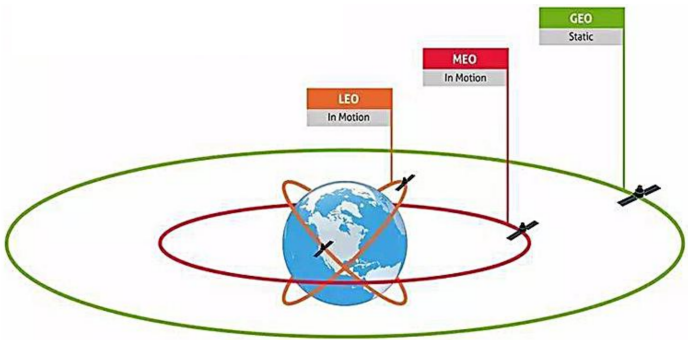


Fig. 6. This illustration depicts the three main satellite orbit types: Low Earth Orbit (LEO), Medium Earth Orbit (MEO), and Geostationary Orbit (GEO). LEO, closest to Earth at altitudes of 500–900 km, features satellites in constant motion, commonly used for Earth observation and communication constellations. MEO, at intermediate altitudes of 5,000–12,000 km, is primarily used for navigation systems such as GPS. GEO, the farthest at 36,000 km, has satellites that appear stationary relative to Earth, making it ideal for communication and weather monitoring.

The propagation time (or delay) for transmissions from satellite to the Earth's surface is primarily determined by the distance between the satellite and the Earth. The following equation can be used to approximate signal propagation time based on the satellite's altitude:

$$t = \frac{h}{c} \quad (16)$$

Where:

- t : Propagation time.
- h : Altitude of the satellite above the Earth's surface.
- c : Speed of light, $c \approx 3 * 10^8 \frac{m}{s}$

The Satellite Communications Toolbox [16] in MATLAB provides functions for the mentioned equations and propagators, which will be employed to simulate the LEO satellite orbit. This simulation will allow us to track the satellite and evaluate the performance of our PID controller.

III. GROUND STATION

A ground station is a land based antenna complex designed for satellite communications, encompassing data transmission, reception and management of telemetry, tracking and payload data as seen in Fig. 7. Ground stations are typically grouped into two categories:

- **Satellite Terminal:** A satellite terminal serves as the user-focused endpoint, positioned at a home, office or any remote location requiring connectivity. These units are engineered to be relatively compact and simple to deploy, meeting the local data demands of households, isolated facilities and mobile platforms such as ships, airplanes or drones. An example of such a terminal is the Starlink antenna, which provides satellite internet access directly to end users.

- **Satellite Gateway:** A satellite gateway functions as a major hub that interconnects satellite networks with broader terrestrial infrastructure for instance the satellite control center in Nemea. It manages and routes extensive volumes of data, enabling robust connectivity for numerous satellite terminals concurrently. These gateways, typically owned by major service providers or enterprises, are often placed in locations that offer minimal interference and ideal line-of-sight to satellites.



Fig. 7. In the left image, a smaller, portable antenna system is shown alongside electronics and a laptop, demonstrating a satellite terminal intended for straightforward deployment in end-user environments. In contrast, the right image showcases Canberra deep space communication complex featuring multiple parabolic dishes, characteristics of a satellite gateway that supports high capacity data links, consolidates traffic from numerous terminals, and interfaces with terrestrial networks to enable robust, large-scale communication.

A. Frequency Spectrum

The transmission of data between a ground station and a satellite relies on radio waves. To effectively penetrate the ionosphere and reach the satellite, these signals operate within the microwave frequency band, typically at frequencies of 1 GHz and above. According to IEEE standard 521-2019 [17], satellite frequency allocations include:

- **L-band (1-2 GHz):** Known for its ability to penetrate weather conditions, making it suitable for GPS and mobile satellite communications.
- **S-band (2-4 GHz):** Commonly used in weather radar and communication satellites.
- **C-band (4-8 GHz):** Resistant to rain fade, making it ideal for satellite television and certain military applications.
- **X-band (8-12 GHz):** Primarily used in radar systems and military satellite communications.
- **Ku-band (12-18 GHz):** Popular for direct broadcast television and high-speed data communications.
- **K-band (18-27 GHz):** Applied in experimental and research satellite links.
- **Ka-band (27-40 GHz):** A newer band with higher data transmission rates, increasingly adopted for satellite constellations and broadband communication.

Fig. 8 illustrates the distribution of these frequency bands, emphasizing the progressive increase in data transmission capacity and the specific advantages for applications as frequencies increase. The Ka-band, representing the high end of this range, is particularly significant for modern satellite

networks, offering enhanced bandwidth and supporting advanced satellite constellations. Operating at such ultra-high frequencies necessitates maintaining a precise line of sight, making accurate satellite tracking essential, particularly for LEO satellites, where rapid movement requires continuous adjustments to ensure reliable communication.

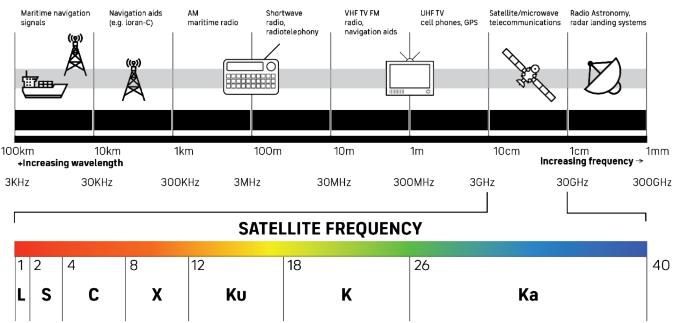


Fig. 8. The figure depicts the electromagnetic spectrum utilized for communication applications, progressing from lower to higher frequencies. It begins with the LF band for maritime and terrestrial communications, followed by VHF and UHF bands for broadcast and early satellite systems. Moving higher, the L-band, S-band, and C-band are used for mobile communication, weather radar, and satellite TV. The X-band and Ku-band serve military and commercial satellites [18], while the K-band and Ka-band enable high-speed broadband and advanced satellite constellations. The color bar represents wavelength variation, transitioning from longer (red) to shorter (blue) wavelengths, corresponding to increasing frequency.

B. Antenna Dynamics

To align the antenna with the satellite, two angles are required: azimuth and elevation. These angles determine the horizontal and vertical positioning of the antenna, as illustrated in Fig. 9, ensuring precise alignment with the satellite's location. This movement is achieved using two DC motors that independently control the azimuth and elevation axes for accurate tracking and positioning.

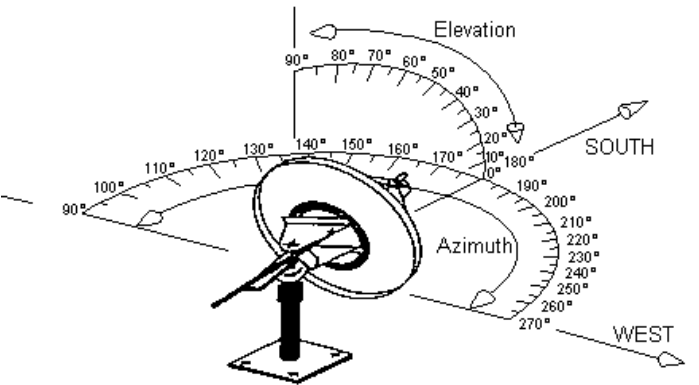


Fig. 9. The figure illustrates the motion of an antenna controlled by two key angles: azimuth and elevation. The azimuth angle governs the horizontal rotation of the antenna, ranging from 0° to 360°, enabling directional alignment relative to compass points (e.g., south and west). The elevation angle defines the vertical tilt, spanning from 0° at the horizon to 90° directly overhead, allowing precise adjustment to align with a satellite at varying altitudes.

C. Effective Beamwidth of the Antenna

Both the satellite and the ground station are equipped with antennas to facilitate communication. A critical parameter to consider when aligning the ground station antenna with the satellite antenna is the beamwidth of the antennas. Antenna beamwidths is defined as the angular range over which most of the antenna radiation is concentrated. It provides a measure of the directional focus or broadness of the antenna's radiation pattern. Typically, the beamwidth is described in terms of the main lobe of the radiation pattern and is measured between the points where the radiation power decreases to half of its maximum value, commonly referred to as the -3 dB points as seen in Fig. 10. Fig. 11 depicts three distinct cases of effective beamwidths commonly encountered in satellite communications.

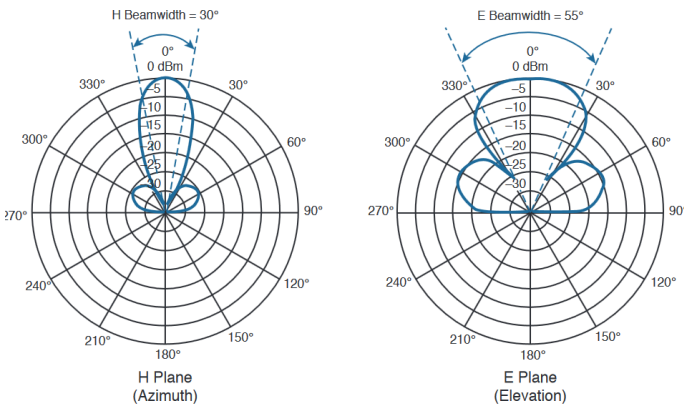


Fig. 10. This image illustrates the radiation patterns of an antenna in both the azimuth (H-plane) and elevation (E-plane). The diagram on the left represents the H-plane, showing a horizontal beamwidth of 30°. This indicates the angular range over which the antenna radiates at least half of its maximum power in the azimuthal direction. The diagram on the right corresponds to the E-plane, depicting a vertical beamwidth of 55°, which describes the angular range for the antenna's radiation in the elevation direction. Both plots are polar diagrams, where the radial axis represents the gain in decibels relative to the maximum power level (0 dBm), and the angular position indicates the direction of radiation. The main lobes, as well as the sidelobes, are clearly visible, providing insights into the antenna's directivity and beamwidth characteristics.

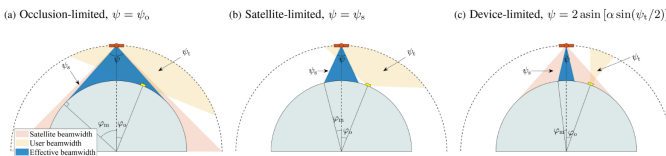


Fig. 11. A satellite-centric representation illustrates the effective beamwidth resulting from the combination of satellite and ground user beamwidths. In scenario (a), both the satellite and the ground user have sufficiently large antenna beamwidths, denoted as ψ_s and ψ_t , respectively. In this case, the effective beamwidth (ψ) between the satellite and the ground station is constrained only by Earth's curvature. In scenario (b), while the ground user has a wide beamwidth, the satellite's beamwidth is relatively narrow, limiting the effective beamwidth to the satellite's beamwidth. Conversely, in scenario (c), the satellite possesses a wide beamwidth, but the ground user's beamwidth is narrow, causing the effective beamwidth to be constrained by the user's beamwidth.

By determining the antenna beamwidths of the satellite and ground station, it is possible to calculate the minimum elevation angle required for the satellite to be accessible by the ground terminal. This calculation is achieved through geometric analysis [19]. The following equation combines the three factors mentioned in Fig. 11 to calculate the effective beamwidth:

$$\psi = \min \left[\psi_s, 2\sin \left(\arcsin \frac{\psi_t}{2} \right) \right] \quad (17)$$

Where:

- ψ : Effective beamwidth.
- ψ_t : Beamwidth of the ground terminal.
- ψ_s : Beamwidth of the satellite.
- $a = \frac{R_e}{R_e+h}$, R_e is the Earth's radius, and h is the satellite altitude.

Based on ψ , we can now calculate the maximum Earth's centered zenith angle:

$$\phi_m = \begin{cases} \arcsin \left(\frac{1}{a} \sin \frac{\psi}{2} \right) - \frac{\psi}{2} & , \psi < \psi_o \\ \arccos(a) & , \psi > \psi_o \end{cases} \quad (18)$$

Where:

- ϕ_m : Maximum Earth's center zenith angle
- $\psi_o = 2\arcsin(a)$, ψ_o is the horizon limiting equivalent angle.

And by plugging Eq. 18 to Eq. 19 we can calculate the minimum elevation angle:

$$El_{min} = \arcsin \left(\frac{\cos(\phi_m) - a}{\sqrt{a^2 + 1 - 2a\cos(\phi_m)}} \right) \quad (19)$$

With Eq. 19, we can effectively evaluate how the selected antenna beamwidths of the satellite and ground terminal influence the satellite pass duration window.

D. Transfer Function of the DC Motor

A DC motor is an electromechanical device that converts direct current (DC) electrical energy into mechanical motion. This conversion is achieved through the interaction of magnetic fields generated by the armature (rotor) and the field windings or permanent magnets (stator). The commutator and brushes facilitate continuous rotation by periodically reversing the current direction in the armature, ensuring consistent torque generation. To mathematically describe the behavior of a DC motor, its transfer function is derived by analyzing both its electrical and mechanical dynamics. A DC motor comprises two primary subsystems, as illustrated in Fig. 12:

- **Electrical System:** Represented by the armature circuit, which governs the electrical dynamics.
- **Mechanical System:** Characterized by the rotational motion of the rotor, which determines the mechanical dynamics.

To derive the transfer function $G(s)$, representing the relationship between the rotor's angular speed ($\omega_m(s)$) and

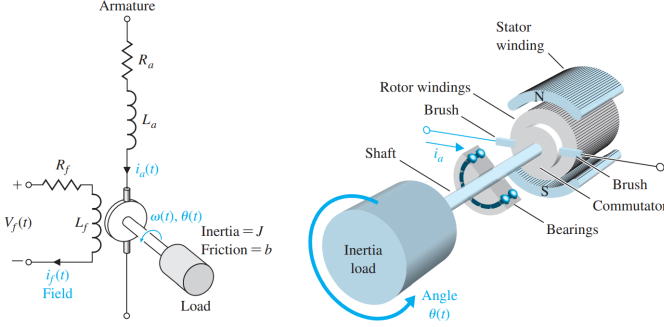


Fig. 12. The figure illustrates the components and operation of a DC motor. The left diagram shows the electrical circuit, including the armature resistance (R_a), inductance (L_a) and current ($i_a(t)$) as well as the field circuit with field resistance (R_f) and voltage ($V_f(t)$). These generate the torque required for motion. The right diagram depicts the mechanical structure, including the rotor, shaft, brushes, commutator, stator, and load. The load's inertia (J) and friction (b) influence the motor's mechanical dynamics, with angular velocity ($\omega(t)$) and position ($\theta(t)$) describing its motion.

the motor's input voltage ($E_a(s)$), the following steps are undertaken:

- 1) **Electrical Dynamics:** Applying Kirchhoff's Voltage Law (KVL) to the armature circuit, we obtain:

$$V_a(t) = L_a \frac{dI_a(t)}{dt} + R_a I_a(t) + e_b(t) \quad (20)$$

Where:

- R_a : Resistance.
- L_a : Inductance.
- $V_a(t)$: Applied armature voltage.
- $I_a(t)$: Armature current.
- $e_b(t)$: Back electromotive force (EMF), proportional to the angular velocity ($\omega(t)$) of the motor:

$$e_b(t) = K_b * \omega(t) \quad (21)$$

Here, K_b is the back EMF constant.

- 2) **Mechanical Dynamics:** The mechanical aspect involves the rotor's moment of inertia (J) and the damping coefficient (B). The torque ($T(t)$) produced by the motor is proportional to the armature current ($I_a(t)$):

$$T(t) = K_t * I_a(t) \quad (22)$$

Where K_t is the torque constant. According to Newton's second law for rotation:

$$T(t) - B * \omega(t) = J * \frac{d\omega(t)}{dt} \quad (23)$$

- 3) **Transfer Function Derivation:** Taking the Laplace transform of Eq. 20 and Eq. 22 (assuming zero initial conditions) and combining them, we derive the transfer function G_s relating the angular velocity ($\omega(s)$) to the input voltage ($V_a(s)$):

$$G(s) = \frac{\omega(s)}{V_a(s)} = \frac{K_t}{(L_a J)s^2 + (R_a J + L_a B)s + (R_a B + K_b K_t)} \quad (24)$$

Where:

a) **Input and Output Variables:**

- $\omega(s)$: Angular velocity of the rotor (output), measured in radians per second (rad/s).
- $V_a(s)$: Applied armature voltage (input), measured in volts (V).

b) **Motor Electrical Parameters:**

- L_a : Armature inductance, measured in henries (H).
- R_a : Armature resistance, measured in ohms (Ω).
- K_b : Back EMF constant, measured in volts per radian per second (V/rad/s).

c) **Motor Mechanical Parameters:**

- J : Moment of inertia of the rotor, measured in kilogram-meter squared ($\text{kg}\cdot\text{m}^2$).
- B : Viscous friction coefficient measured in newton meter second per radian (Nms/rad).
- K_t : Torgue constant, measured in newton meters per ampere (Nm/A).

d) **Components of the Transfer Function:**

- K_t : Represents the motor's ability to generate torque proportional to the armature current.
- $(L_a J)s^2$: Combined electrical and mechanical inertia.
- $(R_a J + L_a B)$: Damping term accounting for electrical resistance and mechanical friction.
- $(R_a B + K_b K_t)$: Steady-state gain and interaction between electrical and mechanical parameters.

Eq. 24 models the dynamic response of a DC motor, allowing for analysis and control system design. For a comprehensive derivation of the transfer function, readers should consult the reference source [20].

E. Proportional Integral Derivative (PID) Controller

In order to track a satellite we will have to give specific voltage inputs to our DC motors to align with the azimuth and elevation of the targeted satellite. To achieve this we need to use a controller and one of the most robust and widely adopted controllers is the Proportional-Integral-Derivative (PID) controller. Its primary objective is to regulate a process variable by minimizing the deviation (error) between the desired setpoint and the system's actual output. The PID controller achieves this through the combined action of three control terms:

- 1) **Proportional Term (P):** The proportional component provides a corrective action directly proportional to the current error:

$$u_P(t) = K_p e(t) \quad (25)$$

Where:

- K_p : Proportional gain.
- $u_P(t)$: Proportional component.
- $e(t)$: Current error at time t defined as $e(t) = r(t) - y(t)$, with $r(t)$ being the setpoint and $y(t)$ the process variable.

This term offers immediate response but cannot eliminate steady-state error on its own.

- 2) **Integral Term (I):** The integral component accumulates past errors to address long-term discrepancies:

$$u_I(t) = K_i \int_0^t e(\tau) d\tau \quad (26)$$

Where:

- $u_I(t)$: Integral component.
- K_i : Integral gain.
- τ : Dummy variable of integration.

By integrating the error over time, it ensures the elimination of steady-state error, albeit at the risk of overshoot and potential instability.

- 3) **Derivative Term (D):** The derivative component anticipates future system behavior by considering the rate of error change:

$$u_D(t) = K_d \frac{de(t)}{dt} \quad (27)$$

Where:

- $u_D(t)$: Derivative component.
- K_d : Derivative gain.

This term provides damping, thereby improving system stability and reducing overshoot, but it is sensitive to measurement noise.

By combining Eq. 25, Eq. 26 and Eq. 27 we can express the PID controller with the following equation:

$$u(t) = K_p e(t) + K_i \int_0^t e(\tau) d\tau + K_d \frac{de(t)}{dt} \quad (28)$$

Where:

- $u(t)$: Control output at time t .
- $e(t)$: Error at time t .
- K_p, K_i, K_d : Gains for proportional, integral, and derivative terms, respectively.

To achieve precise alignment of the antenna with a passing satellite, two PID controllers are utilized: one for azimuth and the other for elevation. By entering the azimuth and elevation of the satellite at time t , these controllers compare the desired values with the output of the system to correct any misalignment. Eq. 28 serves as the foundation for the controller, calculating the alignment error between the antenna and the satellite and applying the necessary corrections to ensure proper alignment as seen in the block diagram of Fig. 13.

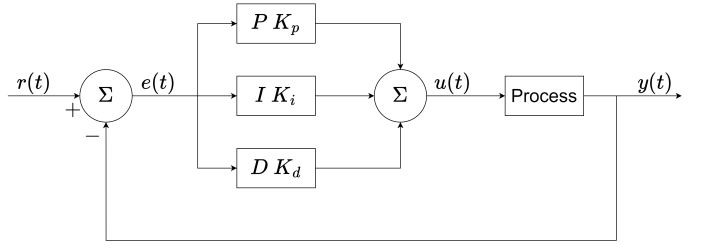


Fig. 13. The block diagram illustrates the proportional (P), integral (I) and derivative (D) control paths acting on the error signal ($e(t)$), which is the difference between the setpoint ($r(t)$) and the process variable ($y(t)$). The weighted outputs (K_p, K_i, K_d) of the P , I and D are summed to generate the control signal ($u(t)$), which is applied to the process to regulate its output ($y(t)$).

IV. SIMULATING THE CONTROL SYSTEM

By integrating the mathematical principles discussed in the previous sections, we can initiate the simulation of the satellite's orbit and implement a PID controller to effectively align the antenna with the satellite's trajectory.

A. Simulating the Satellite's Orbit

The following MATLAB code serves as the computational realization of the mathematical framework described in the Orbital Mechanics section. The objective is to provide a robust and efficient way to analyze and visualize satellite trajectories while validating the mathematical formulations discussed earlier.

First, we define the time vector to simulate the satellite's trajectory. For this specific scenario, we simulate the satellite's motion over a 25-minute period with 1-second intervals, starting from the datetime: 00:00:00 on 4 January 2025. The *satelliteScenario* function, a built-in feature of MATLAB's Satellite Communications Toolbox, generates the time vector, which will be utilized later by our chosen propagator.

This setup ensures that from 00:00:00 to 00:25:00 on 4 January 2025, the satellite's trajectory is computed at 1-second intervals, resulting in 1,500 unique satellite positions. This approach provides a high-resolution simulation to analyze the satellite's behavior over the defined time period.

```

1 %% Create a satellite scenario.
2 startTime = datetime(2025, 1, 4, 0, 0,
3 0);
4 stopTime = startTime + minutes(25);
5 sampleTime = 1;
6 sc = satelliteScenario(startTime,
stopTime, sampleTime);
  
```

Next, we define the ground station, which serves as the base for the satellite tracking antenna. The geographical coordinates for the ground station are specified as follows: {Latitude = 38.12868°, Longitude = 21.74641°, Altitude = 0 meters, Minimum Elevation Angle = 10°}. The *groundStation* function, also a build-in feature of MATLAB's Satellite Communications Toolbox, is used to simulate the ground station at the designated coordinates. In addition to positioning the ground

station, this function also models the local horizon visible to the station while accounting for the antenna's minimum elevation angle. This ensures realistic tracking capabilities by incorporating line-of-sight constraints based on the ground station's geographic location and antenna specifications.

```

1 % Create a ground station to track the
  % satellite and establish an uplink
  % connection.
2 lat = 38.21868;
3 lon = 21.74641;
4 alt = 0;
5 minEl = 10;
6 gs = groundStation(sc, 'Latitude', lat,
  'Longitude', lon, 'Altitude', alt,
  'MinElevationAngle', minEl, 'Name',
  ', "Patras HQ");
```

Finally, we define the Keplerian elements and the propagator for our satellite to generate its trajectory. To ensure the satellite passes over the specified ground station during the defined time vector, we select the following parameters: $\{h = 550 \text{ kms}, e = 0^\circ, i = 40^\circ, \Omega = 10^\circ, \omega = 70^\circ, \theta = 0^\circ\}$. Additionally, the SGP4 algorithm is selected as the propagator to model the satellite's orbit accurately. The *satellite* function, also part of MATLAB's Satellite Communications Toolbox, is used to compute the satellite's trajectory based on the defined Keplerian elements and chosen propagator. This function ensures that the orbital path aligns with the specified parameters, enabling a realistic simulation of the satellite's movement over the defined time period.

```

1 a = earthRadius + 550e3;
2 eccentricity = 0;
3 inclination = 40;
4 RAAN = 10;
5 argofperiapsis = 70;
6 trueanomaly = 0;
7 sat1 = satellite(sc, a, eccentricity,
  inclination, RAAN, argofperiapsis,
  trueanomaly, "Name", "Satellite", "
  OrbitPropagator", "sgp4");
```

Following these procedures, the satellite's trajectory is plotted to enable a comprehensive analysis of its motion. Fig. 14 illustrates the satellite's elevation trajectory, while Fig. 15 depicts its azimuth trajectory. These plots provide critical insights into the satellite's motion, enabling an accurate assessment of its path for further design optimization. Moreover, these visualizations provide the necessary setpoints to be used as inputs to the elevation and azimuth PID controllers.

B. Modeling the PID Controllers

The dynamics of the DC motors are characterized by the parameters listed in Table I. Using the transfer function derived in Eq. 24, two PID controllers were designed and optimized within a closed-loop feedback system using MATLAB's Control System Toolbox [21], as illustrated in Fig. 13. These controllers ensure precise and stable control of the azimuth and elevation motors. The performance of the PID controllers was evaluated by an analysis of the system's step response. For the

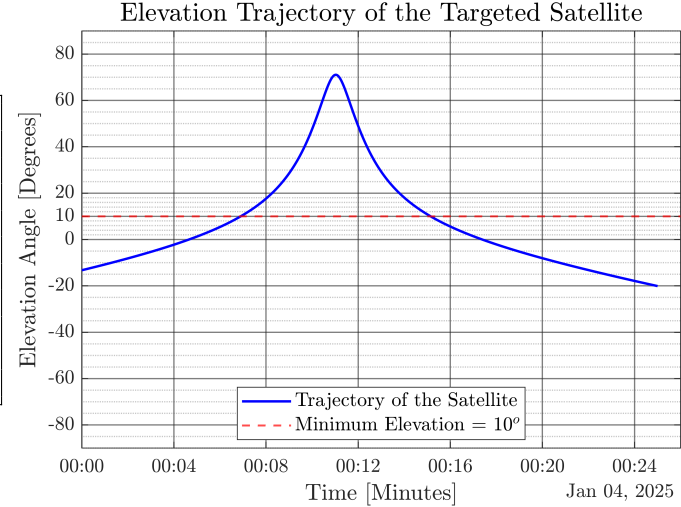


Fig. 14. This plot illustrates the elevation trajectory of a targeted satellite as observed from a ground terminal over a 25-minute period. The y-axis represents the elevation angle in degrees, ranging from -90° to 90° , while the x-axis represents the time duration during the satellite's pass. The blue curve illustrates the satellite's elevation angle over time, peaking as the satellite passes directly overhead. When the blue curve falls below 0° , the satellite is outside the local horizon and no longer visible. The red dashed horizontal line indicates the minimum elevation threshold of 10° , below which the satellite is not visible or trackable by the ground terminal.

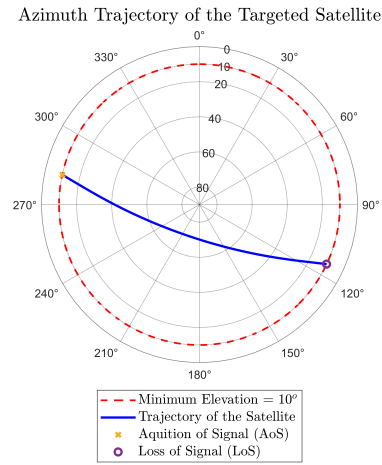


Fig. 15. Polar plot showing the azimuth trajectory of the targeted satellite relative to the ground terminal. The radial axis represents the satellite's elevation angle in degrees (0° to 90°), while the angular axis represents the azimuth angle in degrees (0° to 360°). The blue curve illustrates the satellite's trajectory, demonstrating its elevation and azimuth over time. The red dashed circle marks the minimum elevation threshold of 10° , indicating the minimum elevation angle above which the satellite is visible and trackable by the ground terminal.

given application, achieving a fast rise time and short settling time is critical, while maintaining a low percentage of steady-state error. Figs. 16 and 18 compare the open-loop behavior of the azimuth and elevation motors with the significantly improved closed-loop response achieved using the PID-tuned controllers. Furthermore, Figs. 17 and 19 demonstrate the effectiveness of the PID-tuned controllers in tracking the LEO satellite over the 25-minute time period. These figures compare the setpoint trajectories for azimuth and elevation with the actual responses achieved by the PID controllers, highlighting their precision and accuracy.

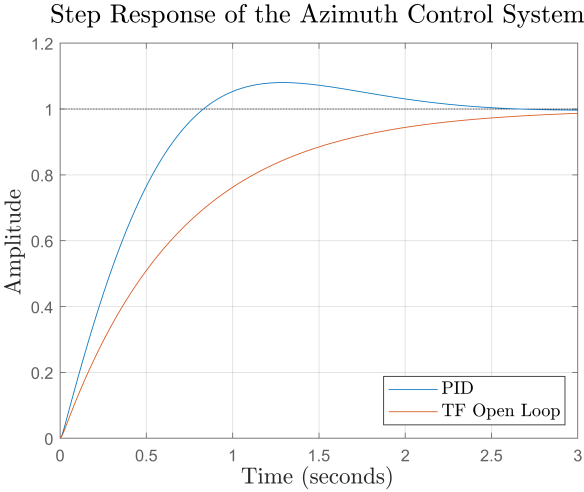


Fig. 16. The figure compares the step response of the azimuth control system in open-loop (orange) and closed-loop (blue) configurations. The PID-tuned closed-loop system achieves a faster rise time, minimal overshoot, and quick settling, while the open-loop response is slower and lacks dynamic regulation. This demonstrates the effectiveness of the PID controller in improving system performance.

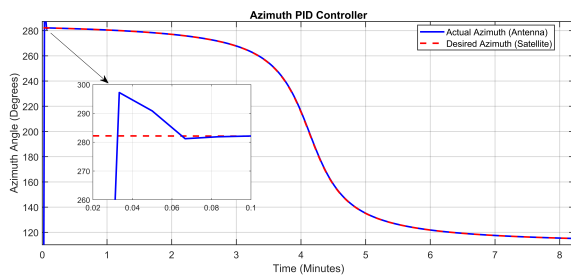


Fig. 17. The figure illustrates the performance of an Azimuth PID controller in aligning an antenna's azimuth angle with the desired satellite azimuth angle. The plot presents the azimuth angle (in degrees) as a function of time (in minutes). The solid blue line represents the actual azimuth angle of the antenna, while the dashed red line corresponds to the desired azimuth angle. The main plot shows that the actual azimuth angle initially deviates from the desired value but converges over time, demonstrating the controller's ability to reduce the error and stabilize the system. An inset plot provides a magnified view of the initial transient response, highlighting the overshoot, settling time, and the early stabilization behavior. This detailed response emphasizes the effectiveness of the PID controller in achieving accurate and stable azimuth alignment with minimal error.

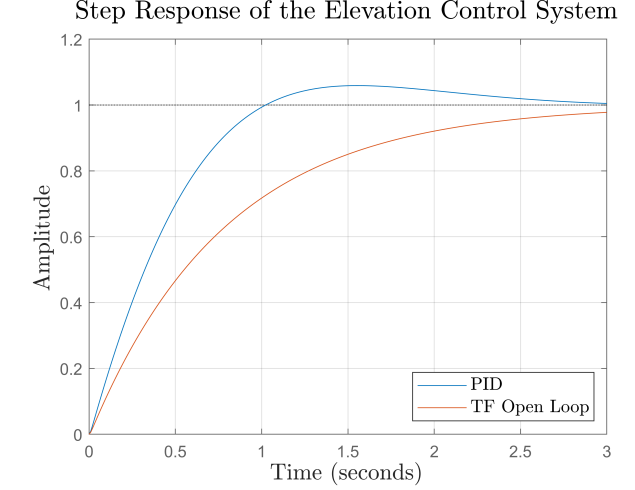


Fig. 18. The figure compares the step response of the elevation control system in open-loop (orange) and closed-loop (blue) configurations. The closed-loop system, tuned with a PID controller, exhibits a significantly faster rise time, minimal overshoot, and rapid settling time. In contrast, the open-loop system demonstrates a slower response with no dynamic regulation, failing to achieve the desired stability and precision. This comparison underscores the effectiveness of the PID controller in enhancing the system's dynamic performance and achieving accurate and stable elevation control.

TABLE I
DC MOTOR PARAMETERS

Definition	Symbol	Azimuth Motor	Elevation Motor	Unit
Torque Constant	K_t	0.45	0.35	Nm/A
Moment of Inertia	J	0.12	0.08	kg * m ²
Damping Coefficient	B	0.06	0.04	Nms/rad
Armature Resistance	R_a	1.8	2.0	Ω
Armature Inductance	L_a	0.015	0.012	H
Back EMF Constant	K_b	0.45	0.35	V * s/rad

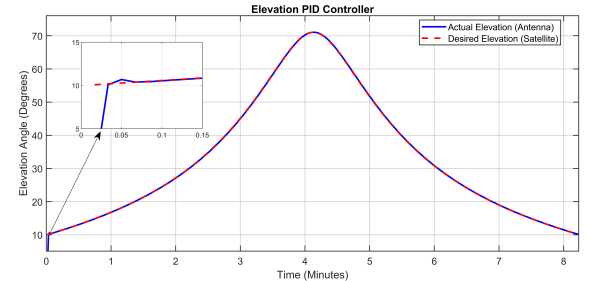


Fig. 19. The figure demonstrates the performance of an Elevation PID controller in aligning an antenna's elevation angle with the desired satellite elevation angle. The elevation angle (in degrees) is plotted against time (in minutes). The solid blue line represents the actual elevation angle of the antenna, while the dashed red line indicates the desired elevation angle. The main plot shows that the actual elevation angle closely follows the desired trajectory, showcasing the controller's ability to maintain accurate tracking throughout the process. Initially, the system exhibits a transient response characterized by a small overshoot and rapid convergence, as highlighted in the inset plot. The inset provides a detailed view of the early response dynamics, illustrating the system's fast stabilization and alignment to the desired elevation. This figure highlights the controller's effectiveness in minimizing error, achieving precise tracking, and maintaining stability over the entire tracking period.

V. CONCLUSION

This paper provided readers with an introduction to orbital mechanics and covered the principles needed to design satellite orbits. It also discussed the types of ground station and presented an approach to LEO satellite tracking using DC motors and PID controller tuning. Finally, a MATLAB simulation tied these concepts together, offering a practical perspective. This work serves as a stepping stone for readers to engage with the complex challenges of mega satellite constellations and deep space missions, a critical issue facing the modern space industry.

REFERENCES

- [1] “4 key areas where AI and IoT are being combined,” Mar. 2021.
- [2] N. Wireless, “Demystifying LEO and its impact on Rural Connectivity,” Mar. 2024.
- [3] “Musk’s Starlink gets Chad go-ahead to improve internet access,” *Reuters*, Nov. 2024.
- [4] “Eutelsat Group Announces Successful Launch of 20 OneWeb Satellites – Company Announcement - FT.com,” Oct. 2024.
- [5] E. Baptista, “China’s Geospace launches 10 low-orbit satellites, eyeing Starlink,” *Reuters*, Sept. 2024.
- [6] A. Staff, “Everything you need to know about Project Kuiper, Amazon’s satellite broadband network,” Mar. 2023.
- [7] “SpaceRISE selected by European Commission to build and operate the IRIS² multi-orbit satellite constellation | SES,” Oct. 2024.
- [8] A. Al-Hourani, “A Tractable Approach for Predicting Pass Duration in Dense Satellite Networks,” *IEEE Communications Letters*, vol. 25, pp. 2698–2702, Aug. 2021.
- [9] “Jonathan’s Space Report | Starlink Launch Statistics.”
- [10] “Starlink,” *Wikipedia*, Nov. 2024.
- [11] “Jonathan’s Space Report | OneWeb Launch Statistics.”
- [12] S. L. Rickman, “Introduction to Orbital Mechanics and Spacecraft Attitudes for Thermal Engineers.”
- [13] “Two-line element set,” *Wikipedia*, Oct. 2024.
- [14] D. Vallado and P. Crawford, “SGP4 Orbit Determination,” in *AIAA/AAS Astrodynamics Specialist Conference and Exhibit*, (Honolulu, Hawaii), American Institute of Aeronautics and Astronautics, Aug. 2008.
- [15] “Types of orbits,” *European Space Agency (ESA)*, Mar. 2020.
- [16] “Satellite communications toolbox,” *MathWorks*, Jan. 2025.
- [17] “IEEE standard letter designations for radar-frequency bands,” *IEEE Std 521-1984*, pp. 1–8, Nov. 1984.
- [18] E. C. Office, “European table of frequency allocations and applications in frequency range 8.3 khz to 3000 ghz,” *European Communications Office*, Mar. 2024.
- [19] B. Al Homssi and A. Al-Hourani, “Optimal Beamwidth and Altitude for Maximal Uplink Coverage in Satellite Networks,” *IEEE Wireless Communications Letters*, vol. 11, pp. 771–775, Apr. 2022.
- [20] R. C. Dorf and R. H. Bishop, *Modern Control Systems*. Hoboken: Pearson, thirteenth edition ed., 2016.
- [21] “Control system toolbox,” *MathWorks*, Jan. 2025.



Ioannis Ziargas is an undergraduate student pursuing a degree in Electrical and Computer Engineering at the University of the Peloponnese. His academic interests focus on telecommunication electronics, with a particular passion for satellite communications. Aspiring to contribute to the space industry, he is driven by the goal of turning his passion into a professional career in this dynamic and innovative field.